

## GRIPPING DEVICES OF INDUSTRIAL ROBOTS FOR MANIPULATING OFFSET DISH ANTENNA BILLETS AND CONTROLLING THEIR SHAPE

Volodymyr SAVKIV<sup>1</sup>, Roman MYKHAILYSHYN<sup>2\*</sup>, Pavlo MARUSCHAK<sup>3#</sup>,  
Valerii KYRYLOVYCH<sup>4</sup>, Frantisek DUCHON<sup>5</sup>, Luboš CHOVANEC<sup>6</sup>

<sup>1,2,3</sup>*Dept of Automation Technological Processes and Production,  
Ternopil Ivan Puluji National Technical University, Ukraine*

<sup>4</sup>*Dept of Automation and Computer-Integrated Technologies named after prof. B. B. Samotokin,  
State University “Zhytomyr Polytechnic”, Ukraine*

<sup>5,6</sup>*Dept of Robotics and Artificial Intelligence, Slovak University of Technology in Bratislava, Slovak Republic*

Submitted 13 May 2020; resubmitted 4 November 2020, 30 November 2020; accepted 31 December 2020

**Abstract.** Invention proposes an adaptive gripping device of an industrial robot, which combines functions of capturing different-shape manipulation objects with control of deviations from the shape of these objects. The device is a T-shaped frame with three Bernoulli grips pivotally mounted thereon and a pneumatic sensor. Analytical dependencies are presented for determination of design parameters of adaptive gripping device and calculation of required lifting force of each of Bernoulli Gripping Device (BGD). Formula is derived for determining its position of pneumatic sensor on frame of gripping devices. In the ANSYS-CFX software environment, numerical simulation of airflow dynamics in the gap between the cooperating BGD surfaces and the offset mirror antenna plate blank. The simulation was based on the Reynolds-Averaged Navier–Stokes (RANS) equations of viscous gas dynamics, the Shear Stress Transport (SST) model of turbulence, and the  $\gamma$  model of laminar–turbulent transition. As a result of the simulation, the effect of the curvature radius of the surface of the plates of offset mirror antennas on the BGD power characteristics was determined.

**Keywords:** Bernoulli gripping device, object manipulation, offset antenna, nozzle, radial flow, industrial robot.

### Notations

BGD – Bernoulli gripping device;  
OM – object of manipulation;  
RANS – Reynolds-averaged Navier–Stokes;  
SST – shear stress transport.

### Introduction

When automating handling operations using industrial robots, the tasks of manipulating articles that change shape during machining often arise. Most often, this problem is solved by cyclic automatic replacement of gripping devices, or as Shameli *et al.* (2007) use magnetic levitation, which generally reduces the productivity of the technological operation. However, there are gripping devices that allow you to gripping objects with different active surfaces. Such gripping devices will reduce the time of transport operations, by using one handling system to grip and hold the part throughout the production cycle. In particular,

pneumatic grippers, namely BGD, have a minimal effect on the lifting force from the curvature of the object to be manipulated.

BGD have a number of advantages – Ozcelik, Erzin-canli (2002) and Ozcelik *et al.* (2003) did research for transportation of non-rigid objects, for transportation of food in production and finished products Davis *et al.* (2008) and Petterson *et al.* (2010), for transportation of skin Dini *et al.* (2009).

A non-contact end-effector was applied by Ozcelik *et al.* (2003) to lift three different materials, which have different physical properties. These materials are mica (as rigid material), carton (as semi-rigid material) and non-rigid material (woven fabric). This end-effector operates on the principle of generating a high-speed air flow between nozzles and the specimen surface thereby creating a vacuum, which levitates the materials with no mechanical contact. In this paper, the handling results of these

\*Corresponding author. E-mail: [mykhailyshyn@tntu.edu.ua](mailto:mykhailyshyn@tntu.edu.ua)

#Editor of the TRANSPORT – the manuscript was handled by one of the Associate Editors, who made all decisions related to the manuscript (including the choice of referees and the ultimate decision on the revision and publishing).

materials are compared with each other. The changes in the physical behaviour of lifting materials were observed during the experimental work. The effect of the various air flow rates on the non-contact handling clearance gap between the nozzle and the materials were also investigated. As a result, it was observed that the non-contact end-effector could be applied to handle different flat materials.

The purpose of paper Petterson *et al.* (2010) is the increase the flexibility of robots used for handling of 3D (food) objects handling by the development and evaluation of a novel 3D BGD. A new gripper technology have been designed and evaluated. A deformable surface have been used to enable individual product handling. The lift force generated and the force exerted on the product during gripping is measured using a material tester instrument. Various products are tested with the gripper. An experimental/theoretical approach is used to explain the results. A deformable surface can be used to generate a lift force using the Bernoulli principle on 3D objects. Using a small forming a significant increase in the lift force generated is recorded. Increasing the forming further was shown to have little or even negative effects. The forces exerted on the product during forming was measured to be sufficiently low to avoid product damage. The improvement of functional and structural integration of the control system components by their integration into the mechatronic module is considered in a paper by Aulin *et al.* (2019).

In paper by Dini *et al.* (2009) proposes the use of contactless grippers instead of more traditional vacuum cups or fingered grippers. In particular, the main objective of this investigation is the measurement of the performance of different gripper configurations whose lifting force is generated by a high-speed air flow passing between the gripper and the leather ply.

Li and Kagawa (2014) investigated the pressure distribution and lifting force of BGD, are measured experimentally. A theoretical model of the air flow between the gripper and the workpiece is created, based on which the theoretical formulas for calculating the pressure distribution and lifting force are derived by Shi and Li (2016). It is found that the outer diameter of the gripper has a major impact on the lifting force, and its design is closely related to the gap height and the supply mass flow rate. Then, the relationship between the outer diameter and the lifting force and that between the gap height and the lifting force are discussed, based on which a method for finding the optimal outer diameter is presented. In paper by Shi and Li (2018) study experimentally and theoretically investigates the dynamic characteristics of the BGD.

It is most of all investigated and introduced on production BGD with cylindrical or circular nozzle and vortex grippers. For the purpose of minimization of energy consumption of BGD when performing handling operations by authors of the paper, the method of optimization of gripper orientation in the course of manipulation was

developed. The method of optimization of BGD orientation when performing transport operations on a rectilinear and arc trajectory is provided by Savkiv *et al.* (2017a, 2017c, 2018b). Influence of force of front resistance of  $Q_1$ ,  $Q_2$  on the minimum necessary lifting force is investigated by Mykhailyshyn *et al.* (2018a). The description of experimental installation and the analysis of the received experimental results on application of a method of optimization of BGD orientation is described by Mykhailyshyn *et al.* (2017).

Gasdynamic analysis of the BGD interaction with the surface of flat objects with displacement of the center of mass carried out by Savkiv *et al.* (2018a) and Maruschak *et al.* (2019). Also the papers by Savkiv *et al.* (2019b, 2017b, 2020a); Mykhailyshyn *et al.* (2019) deals with the topical issue of reducing energy consumption for transportation of industrial objects. The energy efficiency of the process of OM with the use of the orientation optimization method while gripping with the help of different methods has been studied. The economic efficiency of the use of the optimal orientation of BGD while transporting the OM in comparison to the transportation without re-orientation has been proved. Influence of parameters of a gripping system on power expenses of the industrial robot during transportation is investigated Mykhailyshyn *et al.* (2018b).

The advantages of application in the transport and loading systems of gripping devices with the integrated functions of control of parameters of objects of transportation were substantiated in paper by Savkiv *et al.* (2020b). Modelling of BGDs with a possibility of dimensional check and weight OM is offered. Modelling of dynamics of course of air flow in step nozzle and in a radial interval between the interacting flat surfaces of BGDs and OM is carried out. For modelling based on RANS equations of dynamics of viscous gas, SST model of turbulence and  $\gamma$ -model of laminar and turbulent transition are used. As a result of numerical modelling in the program ANSYS-CFX (<https://www.ansys.com/products/fluids/ansys-cfx>) environment operational characteristics of BGD and static characteristic of a measuring nozzle are defined.

In this paper proposed a special gripping device capable of gripping a flat metal sheet for loading into a press, and after it is pressed to grip a blank of a plate of an offset mirror antenna, has acquired a parabolic shape. The main elements of the proposed special gripping device are three Bernoulli grips pivotally mounted on a T-shaped frame. In order to expand the functional capabilities of this gripping device, a pneumatic measuring device is provided in its design. The pneumatic measurement method provides high accuracy and absence of contact with the controlled object, high reliability and durability of operation, ease of automation of the control process. This measuring device allows to perform operational dimensional control of stamped blanks of offset mirror antennas, and to establish deviations from the required geometry.

### 1. Development of the structure and principle of operation of the gripping system

The structure and cross-sections of the individual mechanisms of the device for gripping and controlling the shape of the plates of offset antennas are shown in Figure 1, and the diagram of changing the shape of the antenna blank during stamping in the mold in Figure 2. Gripping device consists of three similar BGD 1, 2, 3 (Figure 1a, 1b, 1c) hinged on T-shaped frame 4. BGD have the possibility of mutual horizontal displacement by means of pins 5 rigidly connected to their upper part, which are aligned with horizontal slots 6 (Figure 1d) of T-shaped frame.

Disk 7 is mounted in each BGD, in axial part of which nozzle 9 is made along normal line to object of processing 8. Two performances 10 and 11 are arranged on different sides of disk 7. The first step 10 in each BGD is arranged around the periphery of the processing object 8, and the second step 11 of each BGD is arranged in series towards the center of the processed object 8. The axis of each pin 5 is perpendicular to the plane passing through the axis of the respective nozzle and the center of the processing object 8.

In the initial state (until the first step 10 enters the radius slot of the blank offset dish antenna 8) with com-

pression spring 14 between the body 15 of the BGD and T-shaped frame 4, the axle 5 together with the body 15 is pressed into the extreme left position of the slot 6 (Figure 1c, 1d). However, the compression spring 16 comprises the housing 15 in its extreme, counter clockwise inclined position defined by the stop 17.

After forming the blank of the offset dish antenna 8 in the mold (Figure 1b), the industrial robot introduces a T-shaped frame 4 into the space above the blank. Positioning of the frame is performed so that the first performance 10 of each of the Bernoulli grippers is set to the lower point of the radial slot of the antenna blank. The robot then performs a further downward shift of the frame, in which each of the Bernoulli grippers is returned to a corresponding angle until contact of the second projection 11 with the antenna blank is reached. At the same time axis 5, is not movably established in building 15 is displaced concerning a groove 6 to the right, the spring 14 and 16 is unclenched at necessary sizes, providing continuity of a kinematic chain from performances 10, 11 to T-shaped frames 4.

After all Bernoulli grippers are installed in the specified position, compressed air is supplied to chamber 12 through channel 13 (Figure 1c). Air flows through nozzle 9 into clearance between lower part of disk 7 and surface of antenna blank. At that, at radius equal to nozzle radius  $r_n$ ,

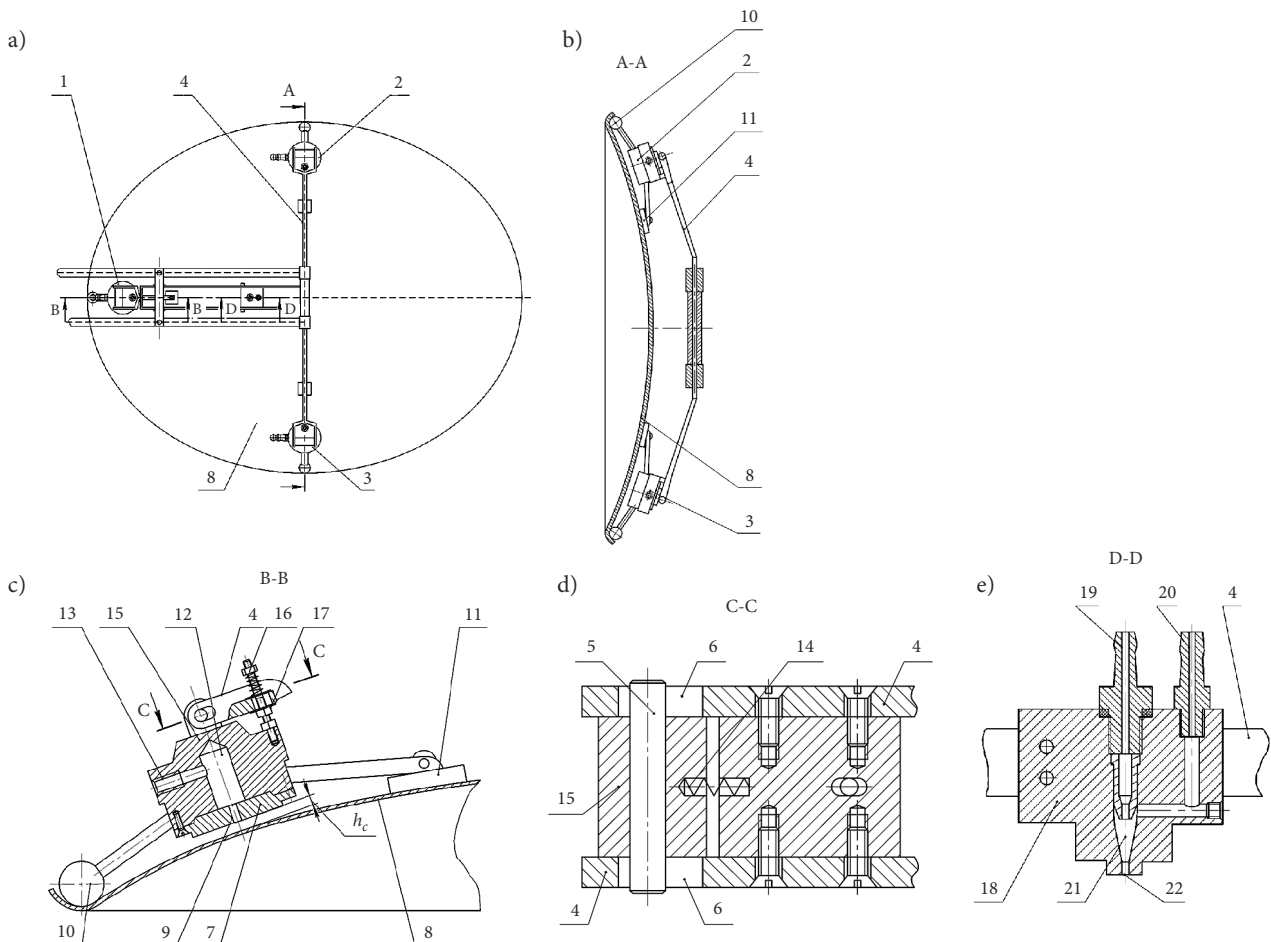


Figure 1. Design and cross-sections of individual mechanisms of the device for gripping and controlling the shape of plates of offset mirror antennas

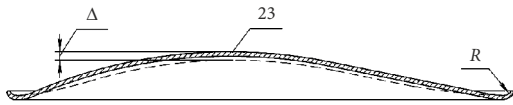


Figure 2. Scheme for changing the shape of offset mirror antenna blank during stamping in a mold

at values of distance between interacting surfaces  $h_c < r_n/2$ , flow experiences greatest narrowing. At the point of greatest narrowing, at excessive supply pressures of the pickup by compressed air more than 30 kPa, the flow reaches the critical speed equal to the speed of sound for these conditions. As a result of further increase of radial flow area, its supersonic speed increases, and static pressure on OM surface decreases to value of lower atmospheric value. At some distance from the nozzle center there is sharp braking of supersonic flow, with its subsequent transition to subsonic flow, which is accompanied by formation of pressure jump. As a result of further expansion, the subsonic flow rate drops and the static pressure in the gap smoothly increases to atmospheric air pressure  $p_a$ . The effect of the vacuum on the surface of the antenna blank results in an lifting force towards the end portion of the disc 7.

Control device 18 (Figure 1e) of this special grip is made in the form of pneumatic size control sensor. It is mounted on the T-shaped frame 4 normal to the offset antenna blank at point 23 (Figure 2), which as a result of the antenna manufacturing process, receives the maximum total strain  $\Delta$ .

Thus, the T-frame is positioned in a well-defined position with respect to the antenna blank. The pneumatic size control device 18 attached to this frame is pre-adjusted to zero count on the offset mirror antenna reference blank with predetermined size parameters. The pneumatic device measures the deviations of the highest point 23 (Figure 2) of the surface profile of the antenna blank relative to the adjusted zero display. This deviation is measured as follows. Compressed air is supplied to measuring chamber 21 under constant inlet pressure through connector 19 (Figure 1e). The air flowing through the measuring nozzle 22 depending on the gap between the end of the measuring nozzle 22 and the surface of the offset mirror antenna blank changes its flow characteristics, thereby changing the air pressure in the measuring chamber 21. The value of this pressure is measured by a sensor, which is connected through a union 20, and after digitization of the measured data, deviation of the profile of the antenna blank is determined. This makes it possible for further transportation of parts to carry out rose backing according to permissible deviation of the outermost point of the profile.

After evaluating the variations in the shape of the antenna blank, the supply of air to the measuring chamber 21 is stopped, and the industrial robot moves the final link upwards. In the following, the industrial robot provides movement of the antenna blank to the unloading zone and stops the supply of compressed air to each of the BGD. Under the action of springs 14, 16 Bernoulli grippers return to initial position.

## 2. Methodology

Using the technique described in paper by Savkiv et al. (2019a), it is possible to determine the pressure distribution in the radial space for the case of interaction of the BGD with the flat surface of the transport object. However, it is quite difficult to analytically evaluate the power interaction of the BGD with the fragment of the parabolic surface of the offset antenna. For this purpose, it is better to use numerical simulation of airflow dynamics in the chamber, nozzles of BGD, and in the interval between its flat surface and the parabolic surface of the antenna blank.

To simulate the airflow between the active surfaces of the BGD and the antenna blank, we will use RANS equations (Snegirjov 2008; Garbaruk et al. 2016). At the same time, the influence of mass forces is neglected. Then the system of basic equations will be as follows:

»» equation of continuity of a stream:

$$\frac{\partial \rho}{\partial t} + \frac{\partial(\rho \cdot V_j)}{\partial x_j} = 0; \quad (1)$$

»» impulse equation:

$$\rho \frac{\partial V_i}{\partial t} + \rho \cdot V_j \frac{\partial V_i}{\partial x_j} = \frac{\partial \tau_{ij}}{\partial x_j}; \quad (2)$$

»» energy equation:

$$\rho \frac{\partial E}{\partial t} + \rho \cdot V_j \frac{\partial E}{\partial x_j} = -\frac{\partial q_j}{\partial x_j} + \frac{\partial}{\partial x_j} (\tau_{ij} \cdot V_i); \quad (3)$$

»» ideal gas state equation:

$$\rho = \frac{p}{R \cdot T}, \quad (4)$$

where:  $i, j$  – indices, take values of 1, 2, 3;  $\rho$  – air density;  $t$  – time;  $x$  – coordinate;  $V$  – vector of air velocity;  $\tau_{ij}$  – stress tensor;  $E$  – the total energy of air;  $q$  – a heat flux density vector taking into account heat transfer by heat conduction and diffusion;  $R$  – gas constant;  $T$  – the absolute air temperature;  $p$  – absolute gas pressure.

The system of Equations (1)–(4) must be supplemented by a turbulence model. The SST is selected to describe turbulence (Menter 1994). The SST model of turbulence is supplemented by transition models Menter et al. (2002, 2006), which allow to predict the position of the laminar–turbulent transition. These models are based on the interleavability coefficient  $\gamma$ , whose value at a given point is determined by the ratio of the flow of which a turbulent mode is observed to the total observation time.

Sufficient accuracy of calculations is given by the laminar–turbulent transition model with another differential equation for the value  $\gamma$  (Menter et al. 2015):

$$\frac{\partial(p \cdot \gamma)}{\partial t} + \frac{\partial(p \cdot V_j \cdot \gamma)}{\partial x_j} = P_\gamma - E_\gamma + \frac{\partial}{\partial x_j} \left( \left( \mu + \frac{\mu_t}{\sigma_\gamma} \right) \frac{\partial \gamma}{\partial x_j} \right), \quad (5)$$

where:  $P_\gamma$ ,  $E_\gamma$  – generative and dissipation members of

managing directors of laminar and turbulent transition, respectively;  $\mu$  – molecular dynamic viscosity of gas;  $\mu_t$  – turbulent dynamic viscosity of gas;  $\sigma_\gamma = 1.0$  – model constant;  $\gamma$  – interleavability coefficient.

The modified equations of the SST turbulence for this  $\gamma$ -model laminar–turbulent transition are as follows (Menter *et al.* 2015):

$$\frac{\partial}{\partial t}(\rho \cdot k) + \frac{\partial}{\partial x_j}(\rho \cdot V_j \cdot k) = \tilde{P}_k + P_k^{\text{lim}} - \tilde{D}_k + \frac{\partial}{\partial x_j} \left( (\mu + \sigma_k \cdot \mu_t) \frac{\partial k}{\partial x_j} \right); \quad (6)$$

$$\frac{\partial}{\partial t}(\rho \cdot \omega) + \frac{\partial}{\partial x_j}(\rho \cdot V_j \cdot \omega) = \alpha \cdot \frac{P_k}{\nu_t} - D_\omega + C \cdot d_\omega + \frac{\partial}{\partial x_j} \left( (\mu + \sigma_\omega \cdot \mu_t) \frac{\partial \omega}{\partial x_j} \right); \quad (7)$$

where:  $k$  – kinetic turbulent energy;  $\omega$  – the specific speed of dissipation of kinetic energy of turbulence;  $P_k$ ,  $D_k$  – original generation and dissipation of the SST model, respectively;  $P_k^{\text{lim}}$  – the additional part, which provides the correct gain of turbulent viscosity in transitional area at very low level of turbulent viscosity of the running stream;  $\nu_t$  – turbulent kinematic viscosity of gas;  $\sigma_k$ ,  $\alpha$  – empirical constants of model; for details and constants see papers by Menter (1994) and Menter *et al.* (2015).

### 3. Analysis of the power characteristics of the BGD

The lifting force by the BGD of the object of transportation is influenced by the following factors: the pressure of supply of the gripping device with compressed air; geometrical parameters of a nozzle; geometric parameters of the surface of the transport object with which the gripping device interacts.

In order to assess the effect of curvature radius (convexities) of fragments of parabolic surface of offset antenna blank on force characteristics of BGDs interacting with these fragments, it is possible to replace parabolic surface with equivalent spherical surface. Such change gives a slight error, since within the fragment of the parabolic surface with which the BGD interacts, the radius of curvature of this surface varies by less than 4%. The radius of curvature of the spherical surface shall be changed within 0.6...3.0 m, which corresponds to the dimensions of offset antennas 0.85...2.15 m.

Numerical simulation of the dynamics of air flow in the chamber, nozzles of the BGD and in the interval between its flat surface and the spherical surface of the object of transportation was performed in the environment of computational hydro-gas-dynamics ANSYS-CFX using RANS and  $\gamma$ -model turbulence. For modelling in this software environment, an unstructured finite difference grid is built in the simulation area. The total number of nodes

in the design area is 2.4...3.2 million. Mesh nodes are combined into three-dimensional elements (tetrahedron and prisms). The total number of volume elements of the grid is 4.6...6.3 million. The total number of tetrahedron is 2.3...3.4 million. In the simulation, it was set: air is the ideal gas; thermodynamic process is adiabatic. The boundary conditions for the airflow model are shown in Figure 3. The simulation was carried out for BGD with nozzle radius  $r_n = 3$  mm and outer radius  $r_g = 30$  mm.

Based on the results of the simulation using the decisive *sonicTurbFoam* module (Menter *et al.* 2006) (for turbulent flows of compressible gases moving at sound and supersonic speeds), graphs of pressure distribution in the interval between the flat end of the BGD and the spherical surface were built for different values of radius  $R$  of this surface at the distance from the nozzle to the spherical surface  $h_c = 0.2$  mm – distance between the interacting surfaces of the OM and the gripping device (Figure 4).

The graphs in Figure 4 show that as the curvature radius of the surface of the OM increases, the size of the supersonic vacuum zone on that surface increases, but the amount of vacuum itself decreases. The radius of curvature of the surface of the OM has minimal influence on the value of the vacuum value in the subsonic zone.

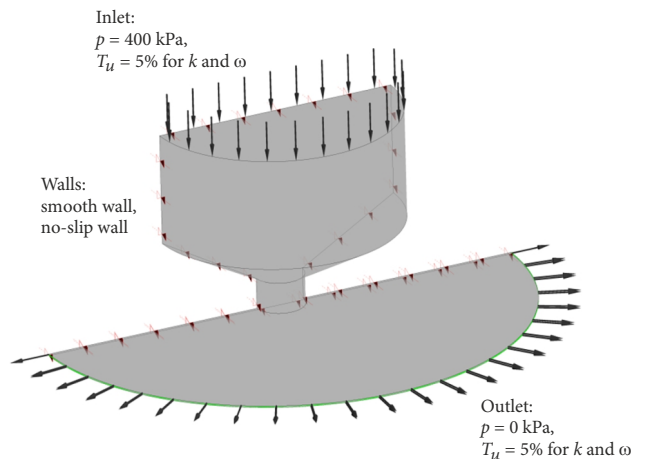


Figure 3. Airflow model limits

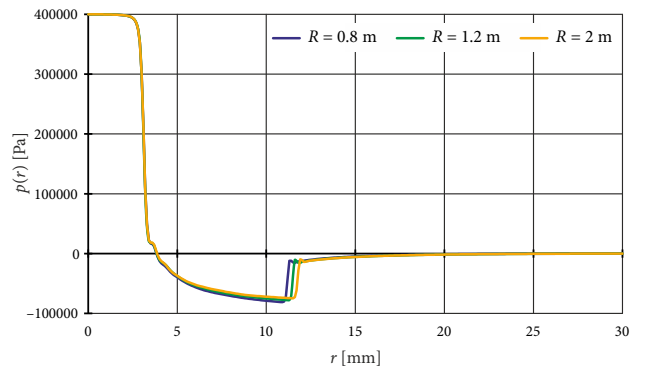


Figure 4. Plots of pressure  $p$  distribution in the interval between the flat end of the BGD and the spherical surface  $r$  for different values of radius  $R$  of this surface

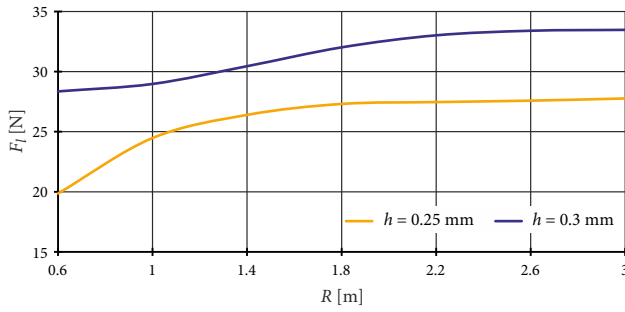


Figure 5. Dependence of the load capacity  $F_l$  of the BGD on the radius  $R$  of curvature of the surface of the content of the transportation object

In order to determine the effect of the curvature radius of the surface of the OM on the carrying capacity of the Bernoulli gripping, numerical integration of the pressure distribution data in the radial gap. As a result, it is revealed that at the radius of curvature of the surface of the OM more than 3 m the lifting force of the BGD reaches the maximum value corresponding to the lifting force of flat objects. It has also been found that when gripping an offset antenna blank with dimensions of 0.85...1.05 m (the minimum radius of curvature of the parabolic surface is 0.6 m), the load capacity of the BGD will decrease by 39% compared to the lifting force of the flat object. The results of the calculations for the two values of the distance between the BGD and the spherical surface are shown in Figure 5.

Analysis of these graphs shows that as the radius of curvature of the surface of the OM increases from 0.6 to 1.8 m, the lifting force of this object by Bernoulli gripper increases by 13...37%, and if the radius increases from 1.8 to 3 m only by 2...4%.

Thus, after determining the required load capacity of BGD 2 and 3 (Figure 1a), appropriate correction is made for increase of their power characteristics depending on diameter of offset antenna blank. The lifting force of the BGD is generally increased by increasing the supply pressure. The main requirement to rational design of BGD is existence of smooth active surface provides smooth narrowing and expansion of airflow and has no performances, which would interfere stream (Wagner et al. 2008). Providing smooth entrance and exit from nozzle reduces losses of energy of air flow and reduces jog force in zone opposite to nozzle (Savkiv et al. 2020a).

By means of additional rotation of the BGD, if there are changes in the shape of the surface of the object to be gripped, it is possible to provide the necessary gap between the lower surface of the disc 7 (Figure 1) and the surface of the object, at which the lifting force of each of the grippers would be maximum.

#### 4. Determination of the power characteristics of the developed handling system

As can be seen from Figure 1a, 1c in static mode, the offset dish antenna blank is sufficient to be held due to the force of only BGD 2 and 3. At the same time BGD 1 is necessary to ensure location of offset mirror antenna blank at its gripping, as well as to prevent antenna rocking at acceleration (braking) of final link operation. Refer to Figure 6 for design diagrams for determining the required lifting force of Bernoulli grippers.

The minimum lifting force of the BGD 2 and 3 (Figure 6) required to contain the stamped antenna blank can be determined from the equilibrium condition of all forces (Figure 6b) acting on this blank at  $N_2 = 0$  ( $N_2$  – normal reaction at the point of contact of the friction element of the handling system). By designing all forces on the  $z$ -axis, we define the condition of antenna blank content:

$$2 \cdot F_l \cdot \cos \alpha > 2 \cdot N_1 \cdot \cos \beta_1 + m \cdot g, \quad (8)$$

where:  $F_l$  – lifting force of gripping device;  $\alpha$  – angle between the vertical and the axis of symmetry of the Bernoulli gripper;  $N_1$  – reaction, acting at the point of contact of the tab 10 (Figure 1) with the surface of the antenna blank;  $\beta_1$  – angle between the vertical and the normal to the tangent to the parabolic surface of the antenna blank at the point of contact of the tab 10 with its surface;  $m$  – antenna mass;  $g$  – acceleration of gravity.

The reaction  $N_1$  can be determined from the BGD equilibrium condition. Taking into account the condition of equilibrium of moments of forces relative to the axis of rotation of the gripping device and the specified condition  $N_2 = 0$ , we will find:

$$N_1 = \frac{F_s \cdot a - m_g \cdot g \cdot b \cdot \sin \alpha}{l_1 \cdot \cos(\alpha - \beta_1)}, \quad (9)$$

where:  $F_s$  is the elastic force of the spring 16 (Figure 1c);  $m_g$  – the mass of the gripping device with stops;  $l_1$  is the

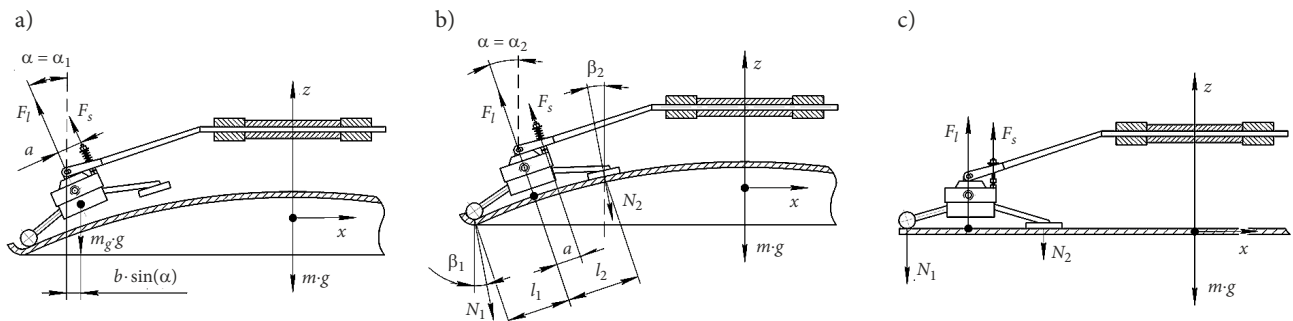


Figure 6. Diagrams for determination of required lifting force of BGD: a – positioning of frame with gripping devices above offset antenna blank; b – grip of offset antenna blank; c – gripping of flat blank

distance from the grip axis to the center of the tab 10 (Figure 6b);  $a$  – the distance between the axis of the Bernoulli gripper and the axis of the applied spring forces;  $b$  – the distance between the axis of rotation and the center of mass of the Bernoulli gripper.

Elastic force of spring 16:

$$F_s = k \cdot \left( \delta_1 + a \cdot (\alpha_1 - \alpha) \cdot \frac{\pi}{180^\circ} \right), \quad (10)$$

where:  $k$  – spring stiffness coefficient;  $\delta_1$  is the value of preliminary compression of spring 16, which provides equilibrium state of BGD at frame positioning above offset antenna blank (Figure 6a);  $\alpha_1$  is angle of inclination of BGD axis, which corresponds to its equilibrium state in initial position.

The initial angle of inclination of the BGD axis is set by the previous compression of the spring 16 so that  $\alpha_1 = \alpha_2 + (5 \dots 7)^\circ$ . Angle value  $\alpha_2$  depends on geometric parameters of offset antenna blank and design parameters of gripping system. The relationship between the value of the spring 16 and its coefficient of elasticity can be determined from Equations (9) and (10), taking into account when positioning the BGD frame above the offset antenna blank (Figure 6)  $N_1$  and  $N_2$  are zero. Then:

$$\delta_1 = \frac{m_g \cdot g \cdot b \cdot \sin \alpha_1}{k \cdot a}. \quad (11)$$

On the basis of Equations (8)–(10), find the required lifting force of BGD 2 and 3 by substituting  $\alpha = \alpha_2$ :

$$F_l > \frac{1}{\cos \alpha_2} \cdot \left( \frac{eq_1}{eq_2} + \frac{m \cdot g}{2} \right), \quad (12)$$

where:

$$eq_1 = k \cdot a \cdot \left( \delta_1 + a \cdot (\alpha_1 - \alpha_2) \cdot \frac{\pi}{180^\circ} \right) - m_g \cdot g \cdot b \cdot \sin \alpha_2;$$

$$eq_2 = l_1 \cdot \cos(\alpha_2 - \beta_1).$$

Find the required lifting force of BGD 2 and 3 for flat blank content (Figure 6c) by substitution  $\alpha = 0, \beta_1 = 0$  in Equation (12):

$$F_l > \frac{k \cdot a}{l_1} \cdot \left( \delta_1 + a \cdot \alpha_1 \cdot \frac{\pi}{180^\circ} \right) + \frac{m \cdot g}{2}. \quad (13)$$

In general, the lifting force by gripping the workpiece can be determined by integrating the absolute pressure distribution  $p_r$  between their cooperating surfaces:

$$F_l = 2 \cdot \pi \cdot \int_0^{r_g} (p_a - p_r) \cdot r dr, \quad (14)$$

where:  $p_a$  – atmospheric pressure.

The lifting force of the handling system  $F_{gs}$  can be determined from Equation (12) by expressing from it the component  $m \cdot g$ :

$$F_{gs} = 2 \cdot F_l \cdot \cos \alpha_2 - \frac{eq_1}{eq_2}, \quad (15)$$

where:

$$eq_1 = 2 \cdot k \cdot a \cdot \left( \delta_1 + a \cdot (\alpha_1 - \alpha_2) \cdot \frac{\pi}{180^\circ} \right) -$$

$$2 \cdot m_g \cdot g \cdot b \cdot \sin \alpha_2;$$

$$eq_2 = l_1 \cdot \cos(\alpha_2 - \beta_1).$$

To analyse the effect of the supply pressure of the Bernoulli grippers on the lifting force of the gripping system, the simulation was performed in the following sequence:

- » using the method presented in parts 2 and 3 of the paper determined the pressure distributions  $p_r$  on the surface of offset antennas (diameters 0.85 and 1.2 m) at supply pressures of Bernoulli grippers 100, 200, 300, and 400 kPa;
- » according to Equation (14), plot the dependence of  $F_l(p)$  (Figure 7a);
- » according to Equation (15), plot the dependence of  $F_{gs}(p)$  (Figure 7b).

Modelling was performed for the following parameters:

- » gripping system:  $r_n = 3$  mm,  $r_g = 30$  mm,  $h_c = 0.25$  mm,  $l_1 = 120$  mm,  $a = 25$  mm,  $b = 40$  mm,  $k = 150$  N/m,  $m_g = 0.3$  kg;
- » an offset antenna with a diameter of 0.85 m:  $a_2 = 14^\circ$ ,  $\delta_1 = 10$  mm;
- » an antenna with a diameter of 1.2 m:  $a_2 = 18^\circ$ ,  $\delta_1 = 12.3$  mm.

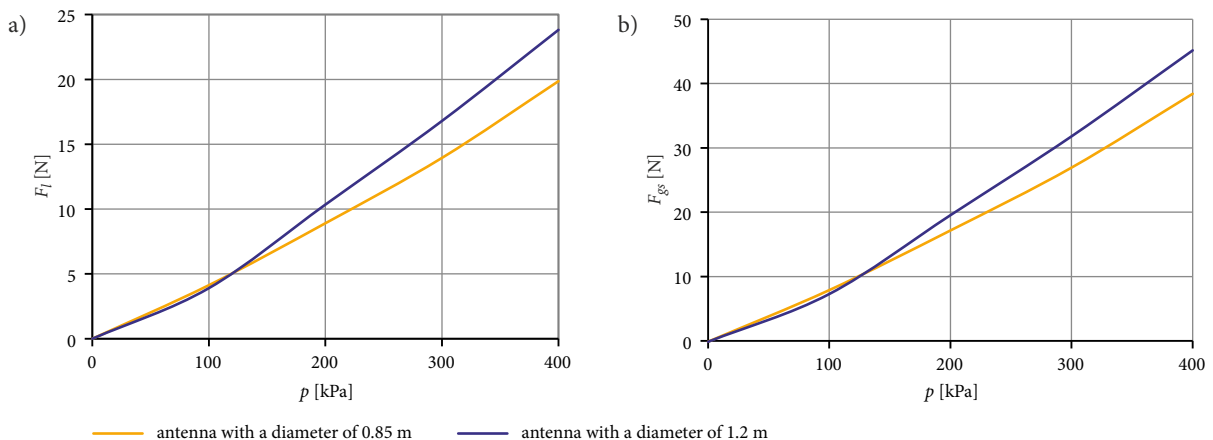


Figure 7. Dependences of the lifting force of offset antennas on the supply pressure: a – one Bernoulli gripper; b – gripping system

Data analysis of Figure 7 shows that the lifting force of the handling system for offset antennas is only 3...7% lower than the total force of interaction of Bernoulli grippers with the surface of these antennas. Prior to that, the lifting force of the handling system based on Bernoulli grippers is decrease with an increased diameter of offset antennas.

## 5. Determining the location of the blank antenna shape control sensor

Formation of elliptical cutting from a paraboloid of rotation is explained by the scheme is submitted in Figure 7. The surface of the offset mirror antenna blank can be represented as being separate from the paraboloid of rotation  $P$  as a result of its crossing by a cutting plane perpendicular to the plane  $XOY$  and returned at an angle  $\theta$  with respect to the axis  $OX$ . The cut plane passes through a point on the paraboloid surface with coordinates  $(x_0, y_0, 0)$  of the original  $XYZ$  system. An elliptical cut in the cutting plane will be formed with a large axis of the ellipse  $L$ , a small axis of the ellipse  $2 \cdot B$ , and the maximum depth  $H$  of the offset antenna blank will correspond to the coordinate  $(x_{pHmax}, H, 0)$ . The maximum elliptical clipping width is  $x_{pBmax}$ .

The specified features of the shape of the working surface of the offset antenna blank define the structural requirements for gripping and the scheme of its dimensional characteristics control. To provide offset mirror antenna with greater spatial stiffness along its contour, radius bend  $R$  is formed (Figure 2). At the same time, depending on the technological conditions of forming the offset antenna blank, there may be a different ratio of plastic and elastic components of deformations for each of the following blanks. This can lead to different changes in the shape of  $\Delta$  caused by instability of the process modes, significantly complicates the task of positioning the invaders on the variable spatial surface of the offset mirror antenna blank. The use of a contactless pneumatic dimensional control sensor in this case is most advantageous, since the probe of the contact measuring tip under the influence of the measuring force can damage the controlled surface.

As the practice of forming offset antennas shows, if the existing shape deviations, they increase sequentially from the periphery of the workpiece to the point of maximum depth of profile  $H$  (Figure 8), that is, point 23 (Figure 2). It is at this point that it is necessary to mount a pneumatic sensor to control the distance from the T-frame to the surface of the workpiece in order to obtain the most complete information about the distortion of the test profile of the workpiece. The coordinates of this point are determined according to the procedure below.

The  $XOY$  plane of the original coordinate system (Figure 8) forms a parabola at the intersection with parabolic  $P$ :

$$x = \frac{y^2}{4 \cdot F}, \quad (16)$$

where:  $F$  is the focus of the parabola.

To form an offset cut, a cut plane is drawn through the  $x_0, y_0$  coordinate point, which extends perpendicular

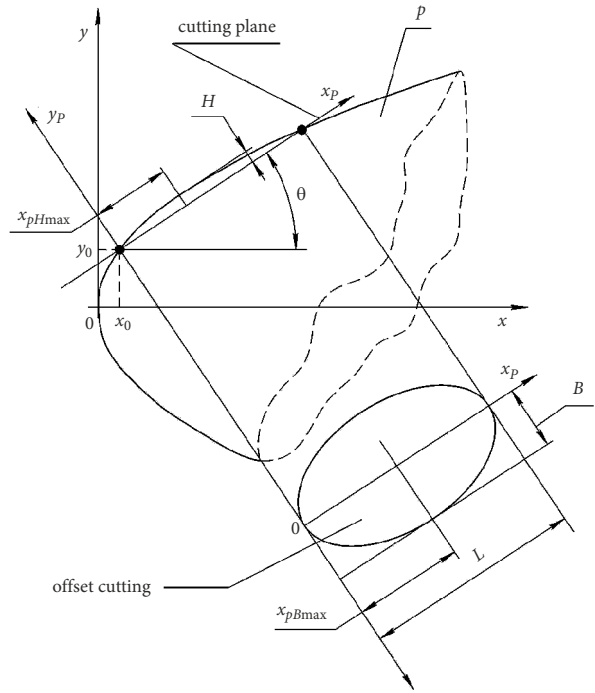


Figure 8. Diagram of elliptical cut-out from parabolic of rotation

to the  $XOY$  plane and is returned at an angle  $\theta$  about the  $OX$  axis. The rotation of the axes in the  $XOY$  plane by the angle  $\theta$  and the transfer of the origin of the reference system in the  $x_0, y_0$  forms the parabola equation in the new system  $x_p, y_p$  as:

$$\begin{cases} x = x_0 + x_p \cdot \cos \theta - y_p \cdot \sin \theta; \\ y = y_0 + x_p \cdot \sin \theta - y_p \cdot \cos \theta, \end{cases} \quad (17)$$

or subject to Equation (16):

$$\begin{cases} \frac{y^2}{4 \cdot F} = x_0 + x_p \cdot \cos \theta - y_p \cdot \sin \theta; \\ y = y_0 + x_p \cdot \sin \theta + y_p \cdot \cos \theta, \end{cases} \quad (18)$$

From the first equation of the system (Equation (18)), the positive value:

$$y = 2 \cdot \sqrt{F \cdot (x_0 + x_p \cdot \cos \theta - y_p \cdot \sin \theta)}. \quad (19)$$

From the second equation of the system (Equation (18)):

$$y = y_0 + x_p \cdot \sin \theta + y_p \cdot \cos \theta. \quad (20)$$

Equating the right parts of Equations (19) and (20) we get:

$$2 \cdot \sqrt{F(x_0 + x_p \cdot \cos \theta - y_p \cdot \sin \theta)} = y_0 + x_p \cdot \sin \theta + y_p \cdot \cos \theta. \quad (21)$$

After converting the Equation (21):

$$\begin{aligned} & y_p^2 \cdot \cos^2 \theta + (4 \cdot F \cdot \sin \theta + 2 \cdot y_0 \cdot \cos \theta + \\ & 2 \cdot x_p \cdot \sin \theta \cdot \cos \theta) \cdot y_p + \\ & (y_0^2 + 2 \cdot y_0 \cdot x_p \cdot \sin \theta + x_p^2 \cdot \sin^2 \theta - \\ & 4 \cdot F \cdot x_0 - 4 \cdot F \cdot x_p \cdot \cos \theta) = 0. \end{aligned} \quad (22)$$

Reduce Equation (22) to the form:

$$y_p^2 \cdot \cos^2 \theta + (4 \cdot F \cdot \sin \theta + 2 \cdot y_0 \cdot \cos \theta + 2 \cdot x_p \cdot \sin \theta \cdot \cos \theta) \cdot y_p + (y_0^2 + 2 \cdot y_0 \cdot x_p \cdot \sin \theta + x_p^2 \cdot \sin^2 \theta - 4 \cdot F \cdot x_0 - 4 \cdot F \cdot x_p \cdot \cos \theta) = 0; \quad (23)$$

$$A \cdot y_p^2 + B \cdot y_p + C = 0, \quad (24)$$

where:

$$\begin{aligned} A &= \cos^2 \theta; \\ B &= 4 \cdot F \cdot \sin \theta + 2 \cdot y_0 \cdot \cos \theta + 2 \cdot x_p \cdot \sin \theta \cdot \cos \theta; \\ C &= y_0^2 + 2 \cdot y_0 \cdot x_p \cdot \sin \theta + x_p^2 \cdot \sin^2 \theta - 4 \cdot F \cdot x_0 - 4 \cdot F \cdot x_p \cdot \cos \theta. \end{aligned} \quad (25)$$

Positive solution of Equation (24):

$$y_p = \frac{-B + \sqrt{B^2 - 4 \cdot A \cdot C}}{2 \cdot A}. \quad (26)$$

The maximum  $y_p$  will be when:

$$\frac{d y_p}{d x_p} = 0. \quad (27)$$

On the basis of Equation (25), taking into account Equation (24), we determine the value of  $x_p$ , which corresponds to the maximum value of  $y_p$ :

$$x_p = \frac{1 - \sin^4 \theta}{\sin^2 \theta \cdot \cos \theta} \cdot F - y_0 \cdot \sin \theta - x_0 \cdot \cos \theta. \quad (28)$$

That is, according to the Equation (28), it is possible to find the installation coordinate of the pneumatic sensor  $x_{pH\max}$  (Figure 8), at which the depth of the cut-out  $H$  will be maximum.

## 6. Analysis of the characteristics of the antenna shape control sensor

Due to the instability of the modes of the technological process of stamping offset antenna blanks and in the course of wear of molds there is a deviation from the reference shape of the antenna. For this type of antenna, this may shift the focal length and impair satellite signal reception. Therefore, it is proposed to use a pneumatic sensor to monitor deviations from the shape of Figure 9.

Modelling of measuring characteristics of the pneumatic sensor was carried out according to the method presented in Section 2 of the paper. The total number of nodes in the design area is 0.05...0.3 million, the total number of volume elements of the grid is 0.3...1.3 million. During the simulation, the following was specified: air is an ideal gas; thermodynamic process is adiabatic. The boundary conditions for the airflow model are presented in Figure 10.

Simulations were performed for a pneumatic sensor with the following parameters:  $d_0 = 0.5$  mm,  $d_1 = 1.6$  mm,  $d_2 = 4$  mm,  $h_c = 0 \dots 0.4$  mm,  $p = 400 \dots 600$  kPa. The results of the pressure distribution along the cross-section of the

measuring nozzle are shown in Figure 11 ( $p = 400$  kPa,  $h_c = 0.2$  mm).

Also, for different values of the radial interval  $h_c$ , the value of the pressure in the channel was determined using a pressure sensor (Figure 9) and the static characteristics of the measuring nozzle were constructed, which are presented in Figure 12.

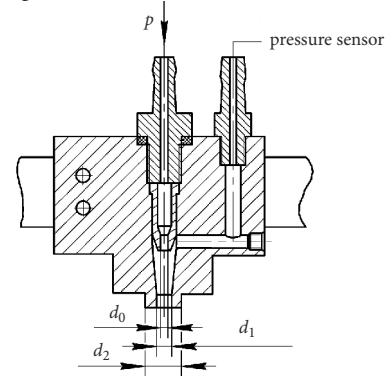


Figure 9. Construction of the antenna shape control sensor:  $d_0$  – diameter of the active nozzle;  $d_1$  – inner diameter of the measuring nozzle;  $d_2$  – outer diameter of the measuring nozzle

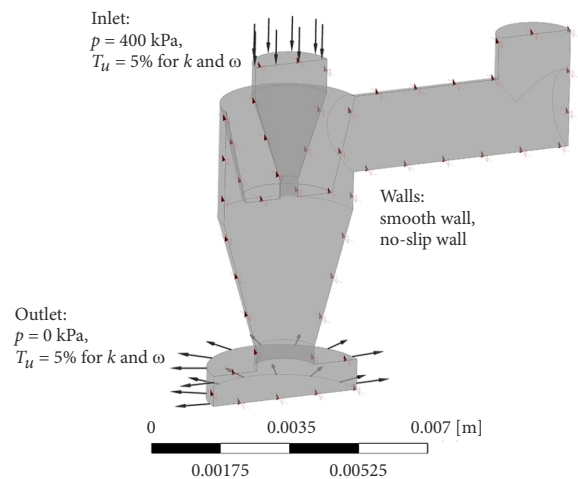


Figure 10. Airflow model limits of the antenna shape control sensor

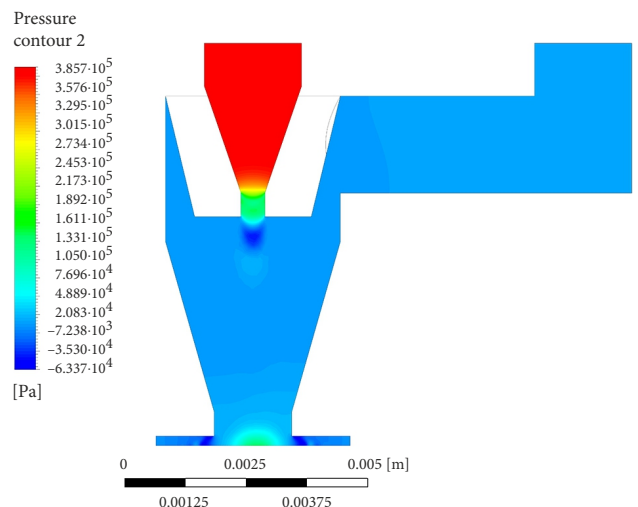


Figure 11. Distribution of pressure along the cross-section of the measuring nozzle

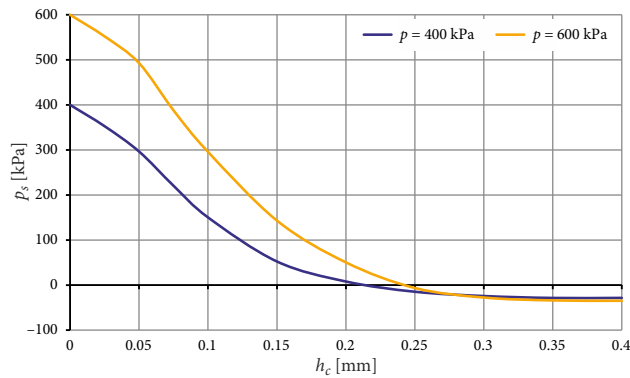


Figure 12. The dependence of the pressure  $p_s$  in the measuring channel of the pneumatic sensor on the distance  $h_c$  to the surface of the antenna

In order to reduce errors in measuring the deviations of the shape of the offset antenna, it is necessary to mount the pneumatic sensor so that the working range of measuring deviations corresponds to the linear section of the dependence  $p_s(h_c)$ , ie the range  $h_c = 0.05 \dots 0.2$  mm. In practice, to ensure high accuracy in measuring the deviations of the shape of the offset antenna, it is necessary to optimize the design parameters of the pneumatic sensor and use a higher level of compressed air supply pressure.

At the same time control of position of the most informative point of the surface of the captured object makes it possible to assess its dimensional characteristics in a comprehensive manner.

The economic effect of the implementation of this device is ensured by the possibility to use it for different processing objects in different form, allows to increase the productivity of the technological process. Savings are also achieved by reducing scrap losses by being able to respond quickly to control results and adjust the process accordingly.

## Conclusions

A BGDs have been proven to allow both flat and objects with convex surfaces to be contained. This allows them to be effectively used as elements of special gripping devices of industrial robots for loading flat metal sheets into the press and unloading stamped plates of offset mirror antennas of parabolic shape.

As a result of the numerical simulation of the dynamics of the airflow in the gap between the interacting BGD surfaces and the plate blank of the offset mirror antenna, it has been found that as the radius of curvature of the surface of the OM increases, the size of the supersonic vacuum zone on this surface increases, but the amount of vacuum itself decreases. It has also been found that the value of the vacuum value in the subsonic zone has a minimal effect on the radius of curvature of the surface of the OM.

With the curvature radius of more than 3 m of OM surfaces, the BGD load capacity reaches the maximum value and approaches the value of the lifting force of the flat

objects. It has also been found that when gripping a blank of an offset antenna with dimensions of 0.85...1.05 m, the load capacity of the BGD will decrease by 39% compared to the lifting force of the flat object.

It is established that the lifting force of the handling system based on Bernoulli grippers decreases with the increasing diameter of offset antennas. The reduction of lifting force occurs only by 3...7% of the total force of interaction of Bernoulli grippers with the antenna surface.

It has been found that the pneumatic sensor for monitoring deviations in the shape of the offset antenna blank must be located at the point of its maximum profile depth. The equation is proposed for the determination of its position of a pneumatic sensor.

The reduction of errors in measuring the deviation of the shape of the offset antenna is achieved due to the operation of the pneumatic sensor on the linear section of its measuring characteristics. This measuring range corresponds to the distance between the pneumatic sensor and the surface of the offset antenna 0.05...0.2 mm.

## Acknowledgements

The results achieved were created in the framework of the projects APVV-17-0214, APVV-16-0006, and “*Robotické pracovisko pre inteligentné zváranie maloobjemovej výroby (IZVAR)*”, code ITMS2014+: 313012P386, co-financed by the European Regional Development Fund.

## Funding

The authors disclosed receipt of the following financial support for the research, authorship of this paper.

This work was supported by APVV-17-0214, APVV-16-0006, and “*Robotické pracovisko pre inteligentné zváranie maloobjemovej výroby (IZVAR)*”, code ITMS2014+: 313012P386, co-financed by the European Regional Development Fund.

## Author contributions

Roman Mykhailyshyn, Volodymyr Savkiv, Valerii Kyrylovych and Frantisek Duchon conceived the research and were responsible for developing and developing data analysis.

Roman Mykhailyshyn, Volodymyr Savkiv, Pavlo Maruschak, Valerii Kyrylovych and Frantisek Duchon were responsible for data collection and analysis.

Roman Mykhailyshyn, Luboš Chovanec and Frantisek Duchon were responsible for modelling in the ANSYS-CFX software environment.

Roman Mykhailyshyn, Pavlo Maruschak and Volodymyr Savkiv wrote the first draft of the paper.

## Disclosure statement

The authors declared no potential conflicts of interest with respect to the research, authorship, and/or publication of this paper.

## References

- Aulin, V. V.; Pankov, A. O.; Zamota, T. M.; Lyashuk, O. L.; Hrynkiv, A. V.; Tykhyi, A. A.; Kuzyk, A. V. 2019. Development of mechatronic module for the seeding control system, *INMATEH – Agricultural Engineering* 59(3): 181–188. <https://doi.org/10.35633/INMATEH-59-20>
- Davis, S.; Gray, J. O.; Caldwell, D. G. 2008. An end effector based on the Bernoulli principle for handling sliced fruit and vegetables, *Robotics and Computer-Integrated Manufacturing* 24(2): 249–257. <https://doi.org/10.1016/j.rcim.2006.11.002>
- Dini, G.; Fantoni, G.; Failli, F. 2009. Grasping leather plies by Bernoulli grippers, *CIRP Annals* 58(1): 21–24. <https://doi.org/10.1016/j.cirp.2009.03.076>
- Garbaruk, A. V.; Strelec, M. H.; Travin, A. K.; Shur, M. L. 2016. *Sovremennye podhody k modelirovaniyu turbulentnosti*. Izdatel'stvo Politehnicheskogo universiteta, Sankt-Peterburg. 234 s. (in Russian). <https://doi.org/10.18720/SPBPU/2/s16-161>
- Li, X.; Kagawa, T. 2014. Theoretical and experimental study of factors affecting the suction force of a Bernoulli gripper, *Journal of Engineering Mechanics* 140(9): 04014066. [https://doi.org/10.1061/\(ASCE\)EM.1943-7889.0000774](https://doi.org/10.1061/(ASCE)EM.1943-7889.0000774)
- Maruschak, P.; Savkiv, V.; Mykhailyshyn, R.; Duchon, F.; Chovanec, L. 2019. The analysis of influence of a nozzle form of the Bernoulli gripping devices on its energy efficiency, in *ICCPT 2019: Current Problems of Transport: Proceedings of the 1st International Scientific Conference*, 28–29 May 2019, Ternopil, Ukraine, 66–74. <https://doi.org/10.5281/zenodo.3387275>
- Menter, F. R. 1994. Two-equation eddy-viscosity turbulence models for engineering applications, *AIAA Journal* 32(8): 1598–1605. <https://doi.org/10.2514/3.12149>
- Menter, F. R.; Esch, T.; Kubacki, S. 2002. Transition modelling based on local variables, in *Engineering Turbulence Modelling and Experiments 5: Proceedings of the 5th International Symposium on Engineering Turbulence Modelling and Measurements*, 16–18 September 2002, Mallorca, Spain, 555–564. <https://doi.org/10.1016/B978-008044114-6/50053-3>
- Menter, F. R.; Langtry, R.; Völker, S. 2006. Transition modelling for general purpose CFD codes, *Flow, Turbulence and Combustion* 77(1–4): 277–303. <https://doi.org/10.1007/s10494-006-9047-1>
- Menter, F. R.; Smirnov, P. E.; Liu, T.; Avancha, R. 2015. A one-equation local correlation-based transition model, *Flow, Turbulence and Combustion* 95(4): 583–619. <https://doi.org/10.1007/s10494-015-9622-4>
- Mykhailyshyn, R.; Savkiv, V.; Duchon, F.; Koloskov, V.; Diahovchenko, I. M. 2018a. Analysis of frontal resistance force influence during manipulation of dimensional objects, in *2018 IEEE 3rd International Conference on Intelligent Energy and Power Systems (IEPS)*, 10–14 September 2018, Kharkiv, Ukraine, 301–305. <https://doi.org/10.1109/IEPS.2018.8559527>
- Mykhailyshyn, R.; Savkiv, V.; Duchon, F.; Koloskov, V.; Diahovchenko, I. M. 2018b. Investigation of the energy consumption on performance of handling operations taking into account parameters of the grasping system, in *2018 IEEE 3rd International Conference on Intelligent Energy and Power Systems (IEPS)*, 10–14 September 2018, Kharkiv, Ukraine, 295–300. <https://doi.org/10.1109/IEPS.2018.8559586>
- Mykhailyshyn, R.; Savkiv, V.; Duchon, F.; Trembach, R.; Diahovchenko, I. M. 2019. Research of energy efficiency of manipulation of dimensional objects with the use of pneumatic gripping devices, in *2019 IEEE 2nd Ukraine Conference on Electrical and Computer Engineering (UKRCON)*, 2–6 July 2019, Lviv, Ukraine, 527–532. <https://doi.org/10.1109/UKRCON.2019.8879957>
- Mykhailyshyn, R.; Savkiv, V.; Mikhalishin, M.; Duchon, F. 2017. Experimental research of the manipulation process by the objects using Bernoulli gripping devices, in *2017 IEEE International Young Scientists Forum on Applied Physics and Engineering (YSF)*, 17–20 October 2017, Lviv, Ukraine, 8–11. <https://doi.org/10.1109/YSF.2017.8126583>
- Ozcelik, B.; Erzincanli, F. 2002. A non-contact end-effector for the handling of garments, *Robotica* 20(4): 447–450. <https://doi.org/10.1017/S0263574702004125>
- Ozcelik, B.; Erzincanli, F.; Findik, F. 2003. Evaluation of handling results of various materials using a non-contact end-effector, *Industrial Robot* 30(4): 363–369. <https://doi.org/10.1108/01439910310479630>
- Pettersson, A.; Ohlsson, T.; Caldwell, D. G.; Davis, S.; Gray, J. O.; Dodd, T. J. 2010. A Bernoulli principle gripper for handling of planar and 3D (food) products, *Industrial Robot* 37(6): 518–526. <https://doi.org/10.1108/01439911011081669>
- Savkiv, V.; Mykhailyshyn, R.; Duchon, F.; Maruschak, P. 2020a. Justification of influence of the form of nozzle and active surface of Bernoulli gripping devices on its operational characteristics, in *TRANSBALTICA XI: Transportation Science and Technology: Proceedings of the International Conference TRANSBALTICA*, 2–3 May 2019, Vilnius, Lithuania, 263–272. [https://doi.org/10.1007/978-3-030-38666-5\\_28](https://doi.org/10.1007/978-3-030-38666-5_28)
- Savkiv, V.; Mykhailyshyn, R.; Duchon, F.; Prentkovskis, O.; Maruschak, P.; Diahovchenko, I. 2020b. Analysis of operational characteristics of pneumatic device of industrial robot for gripping and control of parameters of objects of manipulation, in *TRANSBALTICA XI: Transportation Science and Technology: Proceedings of the International Conference TRANSBALTICA*, 2–3 May 2019, Vilnius, Lithuania, 504–510. [https://doi.org/10.1007/978-3-030-38666-5\\_53](https://doi.org/10.1007/978-3-030-38666-5_53)
- Savkiv, V.; Mykhailyshyn, R.; Duchon, F. 2019a. Gasdynamic analysis of the Bernoulli grippers interaction with the surface of flat objects with displacement of the center of mass, *Vacuum* 159: 524–533. <https://doi.org/10.1016/j.vacuum.2018.11.005>
- Savkiv, V.; Mykhailyshyn, R.; Maruschak, P.; Chovanec, L.; Prada, E.; Virgala, I.; Prentkovskis, O. 2019b. Optimization of Design Parameters of Bernoulli Gripper with an Annular Nozzle, in *Transport Means 2019: Sustainability: Research and Solutions: Proceedings of the 23rd International Scientific Conference*, 2–4 October 2019, Palanga, Lithuania, 423–428.
- Savkiv, V.; Mykhailyshyn, R.; Duchon, F.; Maruschak, P.; Prentkovskis, O. 2018a. Substantiation of Bernoulli grippers parameters at non-contact transportation of objects with a displaced center of mass, in *Transport Means 2018: Proceedings of the 22nd International Scientific Conference*, 3–5 October 2018, Trakai, Lithuania, 3: 1370–1375.
- Savkiv, V.; Mykhailyshyn, R.; Duchon, F.; Mikhalishin, M. 2018b. Modeling of Bernoulli gripping device orientation when manipulating objects along the arc, *International Journal of Advanced Robotic Systems* 15(2): 1729881418762670. <https://doi.org/10.1177/1729881418762670>
- Savkiv, V.; Mykhailyshyn, R.; Duchon, F.; Fendo, O. 2017a. Justification of design and parameters of Bernoulli–vacuum gripping device, *International Journal of Advanced Robotic Systems* 14(6): 1729881417741740. <https://doi.org/10.1177/1729881417741740>
- Savkiv, V.; Mykhailyshyn, R.; Duchon, F.; Mikhalishin, M. 2017b. Energy efficiency analysis of the manipulation process by the

- industrial objects with the use of Bernoulli gripping devices, *Journal of Electrical Engineering* 68(6): 496–502.  
<https://doi.org/10.1515/jee-2017-0087>
- Savkiv, V.; Mykhailyshyn, R.; Fendo, O.; Mykhailyshyn, M. 2017c. Orientation modeling of bernoulli gripper device with off-centered masses of the manipulating object, *Procedia Engineering* 187: 264–271.  
<https://doi.org/10.1016/j.proeng.2017.04.374>
- Shameli, E.; Khamesee, M. B.; Huissoon, J. P. 2007. Nonlinear controller design for a magnetic levitation device, *Microsystem Technologies* 13(8–10): 831–835.  
<https://doi.org/10.1007/s00542-006-0284-y>
- Shi, K.; Li, X. 2018. Experimental and theoretical study of dynamic characteristics of Bernoulli gripper, *Precision Engineering* 52: 323–331.  
<https://doi.org/10.1016/j.precisioneng.2018.01.006>
- Shi, K.; Li, X. 2016. Optimization of outer diameter of Bernoulli gripper, *Experimental Thermal and Fluid Science* 77: 284–294.  
<https://doi.org/10.1016/j.expthermflusci.2016.03.024>
- Snegirjov, A. Ju. 2008. *Vysokoproizvoditel'nye vychislenija v tehničeskoj fizike. Chislennoe modelirovanie turbulentnyh techenij*. Izdatel'stvo Politehnicheskogo universiteta, Sankt-Peterburg. 143 s. (in Russian).  
<https://doi.org/10.18720/SPBPU/2/si20-574>
- Wagner, M.; Chen, X.; Nayerloo, M.; Wang, W.; Chase, J. G. 2008. A novel wall climbing robot based on Bernoulli effect, in *2008 IEEE/ASME International Conference on Mechatronic and Embedded Systems and Applications*, 12–15 October 2008, Beijing, China, 210–215.  
<https://doi.org/10.1109/MESA.2008.4735656>